

On the Estimation of Solar Energetic Particle Injection Timing from Onset Times near Earth

Alejandro Sáiz,^{1,2} Paul Evenson,³ David Ruffolo,¹ and John W. Bieber³

ABSTRACT

We examine the accuracy of a common technique for estimating the start time of solar energetic particle injection based on a linear fit to the observed onset time versus (particle velocity)⁻¹. This is based on a concept that the first arriving particles move directly along the magnetic field with no scattering. We check this by performing numerical simulations of the transport of solar protons between 2 and 2000 MeV from the Sun to the Earth, for several assumptions regarding interplanetary scattering and the duration of particle injection, and analyzing the results using the inverse velocity fit. We find that in most cases, the onset times align close to a straight line as a function of inverse velocity. Despite this, the estimated injection time can be in error by several minutes. Also, the estimated path length can deviate greatly from the actual path length along the interplanetary magnetic field. The major difference between the estimated and actual path lengths implies that the first arriving particles cannot be viewed as moving directly along the interplanetary magnetic field.

Subject headings: Sun: particle emission — interplanetary medium — solar-terrestrial relations — methods: numerical

1. Introduction

An important issue when studying solar events is the exact time when energetic particles are first released from the Sun or its vicinity. This is crucial to understanding the mechanisms

¹Department of Physics, Faculty of Science, Mahidol University, Bangkok 10400, Thailand

²Department of Physics, Faculty of Science, Chulalongkorn University, Bangkok 10330, Thailand

³Bartol Research Institute, University of Delaware, Newark, DE 19716

of particle acceleration and where it takes place (e.g., Kahler et al. 1990). When inferring the start time of particle release, t_0 , one has to take into account the many different processes acting on the particles from their release until the time of detection, t_{onset} , at spacecraft or Earth-based instruments. First the particles (most of them protons) are released with a finite duration of injection at the Sun, and with velocity $v = \beta c$. Because they are charged particles, their motion mostly follows the interplanetary magnetic field, gyrating with a pitch angle θ (defined as the angle between the velocity and the mean field). At the same time, the particles suffer interplanetary scattering due to resonant interactions with magnetic field irregularities leading to a random walk in pitch angle (Jokipii 1966), thus varying the component of the velocity in the direction of the mean magnetic field, $v_z = v \cos \theta$. The random walk can even lead to $\theta > 90^\circ$, which means that particles move back toward the Sun. This leads to a random walk in position as well, and hence to spatial diffusion. There are also effects due to the solar wind speed, such as convection and adiabatic deceleration. These various effects can be taken into account to precisely determine the start time of injection at the Sun (e.g., Bieber et al. 2002, 2004, 2005).

A popular approximation is to consider that the first observed particles move approximately parallel to the mean magnetic field (with $v_z = v$). By doing this one neglects the effects of interplanetary scattering at onset. Then an apparently easy way to estimate the timing is to observe the time of detection onset and shift it according to the path length travelled by the particles. This path length is typically interpreted as the distance along the magnetic field from the Sun to the Earth. Furthermore, when combining measurements at different energies, again under the assumption of no scattering at onset, both the injection time and path length are estimated from a fit of the onset times and inverse velocities to a straight line. This “onset time versus $1/\beta$ ” method has already become a common practice (Lin et al. 1981; Reames et al. 1985; Krucker et al. 1999; Krucker & Lin 2000; Tylka et al. 2003), reinforced by the generally good alignment of experimental data along a straight line in this plot.

However, the basic hypothesis of negligible scattering and motion at zero pitch angle is hard to reconcile with the well-established theories of particle transport. For example, using solutions of a transport equation, Kallenrode & Wibberenz (1990) found that considerable delays in the detected onset can arise both from interplanetary scattering and a finite duration of the particle injection. The onset time can also be affected by other physical processes such as solar wind convection, and also by the technical difficulties in measuring the onset above the pre-event particle background.

Because any major approximation of transport effects must involve some uncertainty, we investigate the validity and systematic error of the approximation that the first arriving

particles have undergone no scattering. We employ state-of-the-art numerical simulations of particle transport, and analyze the resulting onset time versus inverse velocity. We then compare the estimated start time of injection at the Sun and path length with those actually used in the simulation to estimate the systematic error in the estimated values.

Validity of the inverse velocity method was also investigated by Lintunen & Vainio (2004), who considered solar energetic particles of somewhat lower energy. Where they are comparable, our results agree quite well with those presented in their work. In general, we find that the onset time versus $1/\beta$ method, as investigated here for proton energies of 2 MeV to 2 GeV, has a lower timing error than it would if applied to particles of lower energy.

2. Numerical experiments

2.1. Transport model

We describe the propagation of protons ensuing from a solar event by numerically solving a Fokker-Planck equation of pitch-angle transport that includes the effects of interplanetary scattering, adiabatic deceleration and solar wind convection (Roelof 1969; Ruffolo 1995; Nutaro et al. 2001). We are assuming transport along the mean magnetic field, as expected when there is good magnetic connection between the source and the observer. Following Ng & Wong (1979), we define the particle distribution function F depending on time, t ; pitch-angle cosine, μ ; distance from the Sun along the interplanetary magnetic field, z ; and momentum, p , as:

$$F(t, \mu, z, p) \equiv \frac{d^3 N}{dz d\mu dp}, \quad (1)$$

where N represents the number of particles inside a given flux tube. The derived transport equation takes the form:

$$\begin{aligned}
\frac{\partial F(t, \mu, z, p)}{\partial t} = & \\
- \frac{\partial}{\partial z} \mu v F(t, \mu, z, p) & \quad \text{(streaming)} \\
- \frac{\partial}{\partial z} \left(1 - \mu^2 \frac{v^2}{c^2} \right) v_{\text{sw}} \sec \psi F(t, \mu, z, p) & \quad \text{(convection)} \\
- \frac{\partial}{\partial \mu} \frac{v}{2L(z)} \left[1 + \mu \frac{v_{\text{sw}}}{v} \sec \psi - \mu \frac{v_{\text{sw}} v}{c^2} \sec \psi \right] (1 - \mu^2) F(t, \mu, z, p) & \quad \text{(focusing)} \\
+ \frac{\partial}{\partial \mu} v_{\text{sw}} \left(\cos \psi \frac{d}{dr} \sec \psi \right) \mu (1 - \mu^2) F(t, \mu, z, p) & \quad \text{(differential convection)} \\
+ \frac{\partial}{\partial \mu} \frac{\varphi(\mu)}{2} \frac{\partial}{\partial \mu} \left(1 - \mu \frac{v_{\text{sw}} v}{c^2} \sec \psi \right) F(t, \mu, z, p) & \quad \text{(scattering)} \\
+ \frac{\partial}{\partial p} p v_{\text{sw}} \left[\frac{\sec \psi}{2L(z)} (1 - \mu^2) + \cos \psi \frac{d}{dr} (\sec \psi) \mu^2 \right] F(t, \mu, z, p). & \quad \text{(deceleration)}
\end{aligned} \tag{2}$$

Particle velocities are denoted by v , and the solar wind velocity by v_{sw} . The angle between the field line and the radial direction is specified by the function $\psi(z)$, the focusing length by $L(z) = -B/(dB/dz)$, and the pitch-angle scattering coefficient by $\varphi(\mu)$.

In this work, we consider the motion of the particles along a nominal Archimedean spiral magnetic field line (Parker 1958). For this configuration

$$\cos \psi = \frac{R}{\sqrt{r^2 + R^2}}, \quad L = \frac{r(r^2 + R^2)^{3/2}}{R(r^2 + 2R^2)}, \tag{3}$$

where $R = v_{\text{sw}}/(\Omega \sin \theta_H)$, Ω is the angular rotation rate of the Sun and θ_H the heliocentric polar angle, and the radius r can be expressed as a function of z . We consider an equatorial field line ($\theta_H = \pi/2$), a typical value for the solar wind speed ($v_{\text{sw}} = 400 \text{ km s}^{-1}$), and a typical sidereal solar rotation period for magnetic features ($T_{\text{sid}} = 24.92$ days, based on a synodic period of 26.75 days; Bai 1987), so $R = 0.916 \text{ AU}$.

The pitch-angle scattering is parameterized as

$$\varphi(\mu) = A |\mu|^{q-1} (1 - \mu^2). \tag{4}$$

This expression was originally derived in the context of quasi-linear scattering theory (Jokipii 1971; Earl 1973), and here we employ this as a convenient parameterization. The scattering parameter q is taken to be 1.5, which is consistent with values in the range 1.3–1.7 as inferred by Bieber et al. (1986).

The transport equation (2) is solved by means of a finite-difference method (Ruffolo 1995; Nutaro et al. 2001). We consider an initial injection of particles near the Sun with zero pitch angle ($\mu = 1$). Starting from this, simulations provide us with the intensity and anisotropy at any position along the field line and at any time. Thus, we can construct the time profiles for the intensity of energetic protons at the position of Earth’s orbit, for several values of the rigidity P . We consider seven such values, corresponding to kinetic energies of $E = 2, 6, 20, 60, 200, 600,$ and 2000 MeV, that is, from non-relativistic to relativistic proton energies. We consider only the case in which initial intensities follow a power law in rigidity, $I \propto P^{-5}$. An example of the resulting time profiles is depicted in Figure 1.

2.2. Injection profiles

We consider three different cases with different assumptions regarding the rate at which protons are injected into the interplanetary medium from the proximity of the Sun, $I(t)$. Case 1 assumes an impulsive injection (a delta function in time) at $t = t_0$. For Cases 2 and 3, we consider that the injection has a time profile that peaks and decays within a certain time interval. For simplicity, we model this by a triangular profile, starting from $I = 0$ at $t = t_0$, linearly rising to a peak at $t = t_0 + \Delta t$, and linearly returning to $I = 0$ at $t = t_0 + 2\Delta t$. Thus Δt is the full width at half maximum (FWHM) of the injection function. The value of I at the peak is chosen in such a way that the total injected intensity remains the same as in the case of impulsive injection. In Case 2, we assume that the profile has the same width for every value of P ; we take $\text{FWHM} = 12$ min. In Case 3, however, we model the injection by considering different widths for the injection profiles for the different rigidities. As deconvolution techniques have shown that the injection duration tends to decrease with increasing rigidity (Ruffolo et al. 1998; Khumlumlert 2001), for this third case we use values of the FWHM as 75, 50, 30, 20, 12, 8, and 4.8 min., for the seven energy values listed above. Note that in all three cases, the injection is taken to start simultaneously for every rigidity.

2.3. Scattering mean free path

For typical conditions of interplanetary turbulence, the diffusive component of particle transport is characterized by some value of the radial mean free path λ_r on the order of 0.1 to 1 AU. This value varies from event to event, and may also depend on rigidity. We take into account the variability in λ_r by running our simulations with different assumptions for its value: a low constant value $\lambda_r = 0.2$ AU, a high constant value $\lambda_r = 1.0$ AU, or a value depending on rigidity, $\lambda_r \propto P^\alpha$. We explore both positive and negative values of the

exponent, $\alpha = -1/3, 1/3$ and 1 (in addition to the assumptions of constant λ_r , that we can express as cases with $\alpha = 0$). In the rigidity-dependent cases, we fix the value of λ_r for our lowest energy, λ_0 , in such a way that the values for the other energies will roughly remain inside the range 0.2–1.0 AU (see Table 1). As this is not entirely possible for $\alpha = 1$, in this case we use only five energy values instead of seven, thus not considering the relativistic energies $E = 600$ and 2000 MeV.

From quasi-linear theory, one would expect α to be $2 - q$, where q is the power-law index of interplanetary turbulence, also identified with the scattering parameter in equation (4) (Jokipii 1971). For sub-GeV ions that undergo resonant scattering with the inertial range of turbulence, which is observed to have a Kolmogorov spectrum of turbulence with $q = 5/3$ (Jokipii & Coleman 1968), one might expect $\alpha = 1/3$. Most observations favor $\alpha = 0$ to $1/3$ for ions in this energy range (Palmer 1982; Bieber et al. 1994). The other values of α that we consider are applicable to other particle species or ions in other energy ranges. Mean free paths inferred for solar energetic electrons at $P < 2$ MV apparently decrease with increasing rigidity (Dröge 2000), indicating a negative value of α . For ions of roughly 2 to 50 GeV, it is believed that $q \approx 1$ and $\alpha \approx 1$ from various lines of evidence (Leerunnavarat et al. 2003).

2.4. Determination of the onset time

For each particle energy, we can define the time of detected onset, t_{onset} , from the simulated time profiles at Earth orbit, as the moment when these profiles surpass a certain threshold value. In the case of a real event, this threshold would arise from the mean background level prior to the protons’ arrival, and its fluctuations. However, there is a large variability in the proton background and energy spectrum before each solar event: the background may either depend on the level of galactic cosmic rays or be an advanced phase of a previous solar particle event. For our purposes, we define the threshold to be a constant fraction of the maximum intensity at each energy value. We explore the cases in which the onset times are determined by assuming a low threshold, corresponding to a constant fraction of 0.01% of the peak, a medium threshold, at 2% of the peak, or a high threshold, at 60% of the peak (see Figure 1).

From the point of view of observations, a high threshold like 60% of the peak would be the case when the pre-event background is very high (e.g., when a new event occurs in the decay of a previous event), or for very small events. Such events are not usually included in practical onset time analyses. When conditions are favorable for observations, event onsets can be detected at thresholds similar to our medium threshold (2% of the peak). Detection at a low threshold like 0.01% of the peak would be unusual, but we include this case in order

to explore the systematic errors of the inverse velocity method in the limit of very good observation conditions.

3. Inverse velocity fits

The estimation technique examined in this paper assumes that the first detection of protons at a given energy occurs for those protons arriving at their maximum velocity along the field line, which would be consistent with the supposition that particles with roughly zero pitch angle ($\mu \simeq 1$) would suffer negligible scattering. If this holds, then t_{onset} as a function of the particle velocity follows the simple relation

$$t_{\text{onset}} = t_{\text{inj}} + \frac{s}{v}, \quad (5)$$

where t_{inj} is the time when the injection starts and s is the path length travelled by the particles. These last two parameters can be tuned to fit the data points to the expression in equation (5), which gives a straight line in the t_{onset} vs. $1/v$ plot.

Three examples of the inverse velocity fit are shown in Figure 2. We see that the injection time deduced this way (the y -intercept of the best-fit line) is slightly late with respect to the actual injection start time ($t = t_0$) and that the path length (the straight line’s slope) is longer than the actual field line length of 1.16 AU.

The results of the inverse velocity fits for all the cases studied in this paper are summarized in Table 1 and plotted in Figure 3. As can be seen, in most of the cases the fits for the low threshold definition of t_{onset} yield an injection time that is correct to within a few minutes and a high value of the path length. For the higher threshold assumptions, the trends are similar but with increased deviations from the correct values. Our results are similar to those found by Lintunen & Vainio (2004) for simulated events of solar energetic protons with energies 1–57 MeV. However, these authors found much higher deviations (even of hours) in the estimated injection times when considering cases with both lower proton energies (down to 130 keV) and very short mean free paths (cases that would correspond to $\lambda_0 \lesssim 0.1$ AU).

It is worth to note that, although the range of energies that we use throughout this work, i.e., 2–2000 MeV, is comparable to the high-energy channels studied by Lintunen & Vainio (2004), i.e., 1–57 MeV, these authors considered only one type of high-energy dependence of λ_r with P , that corresponds to our case of $\alpha = 1/3$. This leaves only one case, among the cases studied by those authors, with which we can compare directly the results of the present work, i.e., the one with a normalization in the λ_r dependence that is consistent with

the one used here (see Table 1), which is their case no. 5, normalized to have $\lambda_r = 0.5$ AU at $P = 1$ GV. Our results indicate a deviation in the injection time of -0.99 min and a path length of 1.32 AU (when assuming a threshold of 0.01% of the peak), which compares well with their values, -1.7 ± 0.4 min and 1.33 AU (for a threshold of 0.1% of the peak).

We now study how the different simulation parameters affect the estimated parameters t_{inj} and s . For example, regarding the injection profile, we observe that the trend is similar for each mean free path assumption: if the injection is extended and of constant width (FWHM = 12 min), the derived injection time, t_{inj} , is always later than in the impulsive injection case, and the path length, s , changes slightly. When the width of the injection profile varies, with broader injections for lower rigidities, t_{inj} is usually slightly later but not far from the impulsive injection case. On the other hand, derived s values are systematically longer. These differences for different injection assumptions also increase for the higher threshold assumptions. Our results are consistent with those of Lintunen & Vainio (2004), who studied only the effects of an extended injection with constant width, and who also found a delay in derived injection times and slightly longer path lengths. The results are qualitatively the same, although these authors used a much longer injection (FWHM ≥ 3.7 h) and a “top-hat” profile.

As previously mentioned, the injection time, t_{inj} , is usually not far from the time of injection used in the simulations, t_0 , but we observe that simulation results for the case in which the scattering mean free path decreases with rigidity (negative α) tend to give later injection times while the cases for λ increasing with rigidity (positive α) tend to give earlier injection times. This is particularly extreme for $\alpha = 1$, a case of strong dependence.

The estimated path length, s , for an impulsive injection seems to depend mainly on the value of the mean free path at the lowest energy. This is because the point corresponding to the onset of the slowest particles will have a higher relative weight in the t_{onset} vs. $1/v$ fit. This is also apparent in the results of Lintunen & Vainio (2004, their Table 2 and Figure 3), though not explicitly discussed in that work. In cases where a different low-energy dependence of λ_r with P resulted in a similar value of λ_r for the lowest energy value (e.g., their cases 6 and 13), the resulting value of s was similar.

An interesting result is that while many of the simulations yield estimated t_{inj} and s values with substantial errors, all the simulations are nevertheless well fit by straight lines in t_{onset} versus $1/v$. The worst fit of all is included in Figure 2 (indicated by triangles), and to the eye even this appears quite good. (Actual observations would involve some fluctuations, which may even dominate the deviations shown here.) Yet according to Figure 3, some of these apparently good fits yield path lengths over 2 times too long or injection time errors of over 10 minutes. Thus the goodness of fit alone does not validate the results or assumptions

of the inverse velocity fits.

To quantitatively compare the various fits, it is interesting to examine the unweighted χ^2 function,

$$\chi^2 = \sum_{i=1}^N \left[t_{\text{onset},i} - \left(t_{\text{inj}} + \frac{s}{v_i} \right) \right]^2. \quad (6)$$

We can regard this not only as an estimation of the goodness of the fit but also as a measure of the departure of our “experimental data” from the linear relation. In Table 1 we show the value of χ^2 divided by the number of degrees of freedom, $N - 2$, with N as the number of data points. We find that the worst fits are mostly among the cases of strong dependence of λ_r with rigidity, that is, for $\alpha = 1$ and $-1/3$, although there are exceptions. On the other hand, one of the best fits, which is also the point appearing closest to the correct values in Figure 3, is that corresponding to an impulsive injection and a high constant mean free path, $\lambda_r = 1.0$ AU. This is actually the set of parameters closest to those that would fulfill Eq. (5) exactly (in the absence of solar wind convection) for any threshold, that is, an impulsive injection with a mean free path $\lambda_r \rightarrow \infty$.

Although all of the linear fits are good, it is interesting to note that a very good fit, or even the best fit (depending on the threshold assumption), corresponds to the case for which λ_r increases with rigidity as P^α with $\alpha = 1/3$. This very good alignment arises from offsetting effects of the variable λ_r and the solar wind convection, the former favoring the transport of faster particles and the latter having a greater relative importance for slower particles. [Note also that $\alpha = 1/3$ would arise from quasi-linear theory with a Kolmogorov spectrum of magnetic fluctuations (Jokipii 1971) and is also supported observationally (e.g., Valdés-Galicia et al. 1995) and theoretically (e.g., Bieber et al. 1994).] However, even in this case, the fit parameters differ considerably from the correct values, especially the path length of 1.3–1.7 AU, depending on the threshold. This means that for typical values of the solar wind speed, the interplanetary turbulence effects on the transport of particles of different energies can produce onset times near Earth that align extremely well in the inverse velocity plot, but whose fit leads to a value of the path length 20–50% longer than the actual length of the field line.

This may explain some of the results of Tylka et al. (2003), who found long path lengths in some events analyzed using the onset time versus $1/\beta$ method. They included measurements of protons, ions, and electrons for $1/\beta$ values of $\simeq 1$ –15, which for protons corresponds to energies from $\simeq 2$ MeV to several GeV. Using this method they found, e.g., a path length of 1.36 ± 0.02 AU for the impulsive event of May 1, 2001, and a path length of 1.67 ± 0.02 AU for the ground level event of April 15, 2001. This last event (known as the Easter 2001 event) was also studied by Bieber et al. (2004), who found a good fit to neutron

monitor data by using a detailed treatment of interplanetary transport (as described in §2.1) and a magnetic field line length of approximately 1.2 AU, as expected given the value of v_{sw} during that event. We have performed a similar analysis under the supposition of a path length of 1.7 AU, but in this case the fit to the data is quite poor, with a value of χ^2 per degree of freedom that is roughly 9 times larger than that found by Bieber et al. (2004) for 1.2 AU. Note that the injection start times derived by Tylka et al. (2003) and Bieber et al. (2004) agree to within 3 minutes. The small difference in injection time and major difference in path length is entirely consistent with the results of the present work.

4. Implications for solar electrons

The study of solar energetic electrons is of special interest in understanding particle emission and transport in solar events. The propagation of solar electrons can be tracked by Type III radio emission (Reiner & Stone 1988, 1989) and has been shown to be closely related to the propagation of ions (Cane & Erickson 2003). In addition, electron onset times are generally detected with better accuracy than for ions, and are also used to infer injection times through the inverse velocity method (e.g., Lin et al. 1981; Krucker et al. 1999).

Although in the present work we focus on the transport of solar protons, the question arises at this point about whether the results of §3 can be applied to solar electrons as well. Our answer is yes. The transport of solar energetic particles along the magnetic field line that connects the acceleration site to the observer does not depend on the particles' mass or the sign of their electric charge. It does depend on their velocities, on the interplanetary scattering conditions, and to a lesser extent, on the spectral index of particle emission, see equation (2). Therefore, the results presented above are applicable, under the same assumptions regarding scattering mean free paths λ_r and injection profiles, to solar electrons of similar velocities as the seven values used for protons, which correspond, roughly speaking, to electron energies of $E = 1, 3, 10, 30, 100, 300,$ and 1000 keV. This range of energies is also compatible with most solar energetic electron observations.

From these considerations, we also conclude that the onset analysis of electrons and ions for the same event may lead to differences in the fit parameters that would arise from differences in λ_r , in the injection duration, or in the threshold for detecting the onset. It has been shown (Bieber et al. 1994, especially Figure 3) that the electron and proton mean free paths are similar in the same event for a range of mean free paths over two orders of magnitude. Even if we consider that the value of λ_r is exactly the same, the inverse velocity method will give different results for protons and electrons if their injection durations are different. If, for example, the injection is impulsive for electrons but extended with constant

width for protons, and both injections start simultaneously, the fits will estimate a later t_{inj} for protons than for electrons, and approximately the same s . Under the same conditions except that the injection duration for protons depends on rigidity as proposed in §2.2, the resulting t_{inj} will be similar in both fits but s will be longer for protons. Further deviations may arise from differences in the rigidity dependence of λ_r . The results of Dröge (2000) suggest that the mean free path varies smoothly with rigidity from electrons at low rigidity to protons at higher rigidity for the same event, but changes its dependence with rigidity, with negative α for electrons and positive α for protons. According to our results, this effect would add an extra difference in s between protons and electrons, with longer s for protons. We refer the reader to Table 1 for other possible combinations. In summary, the inverse velocity method may introduce artificial differences in estimated injection times and especially path lengths when used with electrons and protons for the same event (e.g., Krucker & Lin 2000).

5. Discussion and Conclusions

The results of the pitch-angle transport simulations are not compatible with the assumption of no scattering for the first detected particles. We find that the onset time for each energy is always influenced by interplanetary scattering, the duration of injection, and solar wind convection, each of which may have a different relative importance for different energies. The onset delays found for single energy values are consistent with Kallenrode & Wibberenz (1990), who used a focused transport equation but did not include any effects of the solar wind speed.

By combining the onset times at different energies in the inverse-velocity plot, a simple fit leads to an estimation of the start time of the injection, t_{inj} , and the path length, s , with results comparable to those of Lintunen & Vainio (2004). We find that often a good linear fit is obtained fortuitously, even when the fit parameters deviate substantially from the true values. Thus the goodness of the fit should not be taken as an indication that the estimated values or underlying assumptions are correct.

While Lintunen & Vainio (2004) found some cases with a major error in the timing estimation (even of hours), this was never the case when they considered only proton energies greater than 1 MeV. We do not find deviations in the timing estimation larger than several minutes in our results for protons of 2 MeV to 2 GeV, or electrons of 1 keV to 1 MeV. We note that most practical applications of this estimation technique (e.g., Lin et al. 1981; Reames et al. 1985; Krucker et al. 1999; Tylka et al. 2003) have considered values of $1/\beta$ up to only 10 or 20, corresponding to proton energies larger than 1 MeV, or electron energies

larger than 500 eV. In such cases, the onset time versus $1/\beta$ method is unlikely to incur timing errors greater than several minutes.

It should be noted that fits to intensity and anisotropy data of solar energetic particles using detailed transport modeling can yield a complete injection function, not only the start time of injection. Such information can be derived for each energy, as well as the mean free path and magnetic configuration (Ruffolo et al. 1998; Bieber et al. 2002). On the other hand, although the use of inverse-velocity fits is based on a highly simplified assumption for interplanetary transport, it often results in roughly correct start times of injection, with typical errors of several minutes, as long as the interplanetary scattering is not excessively high.

In contrast, the path lengths obtained from the linear fits are frequently very different from the actual path length along the local interplanetary magnetic field line, and always larger. This clearly indicates that the first arriving particles cannot be viewed as moving directly along the interplanetary magnetic field, with $v_z = v$ and zero pitch angle. Empirically, a better assumption would be that the first arriving particles travel with an energy-independent value of the pitch angle cosine, $\mu = v_z/v$, that is less than unity. Indeed, this is a feature of the coherent pulse concept of focused transport theory (Earl 1976a,b) for a scattering mean free path that depends only weakly on energy. Figure 2 would seem to imply that higher thresholds (relative to the peak) represent the arrival of particles with decreasing μ . For a path length z , the “onset” particles empirically arrive roughly at time

$$t_{\text{onset}} = t_{\text{inj}} + \frac{z}{v_z} = t_{\text{inj}} + \frac{s}{v}, \quad (7)$$

where $s = z/\mu$ for an unknown value of μ that is apparently roughly constant with energy. The coherent pulse concept can help explain why the inverse velocity fits provide estimates of s that do not represent the actual path length, but rather the path length magnified by some factor ($1/\mu$), and estimates of the start time of injection that are accurate to the order of several minutes.

This work is based on a presentation to the ACE/RHESSI/WIND Workshop in Taos, NM on October 8, 2003. The authors acknowledge useful discussions at the 2003 SHINE Workshop and with A. Tylka. We thank P. Wongpan for his assistance. This work was partially supported by the Thailand Research Fund, the Rachadapisek Sompoj Fund of Chulalongkorn University, and the US National Science Foundation (award ATM-0000315).

REFERENCES

- Bai, T. 1987, *ApJ*, 314, 795
- Bieber, J. W., Clem, J., Evenson, P., Pyle, R., Ruffolo, D., & Sáiz, A. 2005, *Geophys. Res. Lett.*, 32, L03S02
- Bieber, J. W., Evenson, P. A., Dröge, W., Pyle, R., Ruffolo, D., Rujiwarodom, M., Tooprakai, P., & Khumlumlert, T. 2004, *ApJ*, 601, L103
- Bieber, J. W., Evenson, P. A., & Pomerantz, M. A. 1986, *J. Geophys. Res.*, 91, 8713
- Bieber, J. W., Matthaeus, W. H., Smith, C. W., Wanner, W., Kallenrode, M.-B., & Wibberenz, G. 1994, *ApJ*, 420, 294
- Bieber, J. W. et al. 2002, *ApJ*, 567, 622
- Cane, H. V. & Erickson, W. C. 2003, *J. Geophys. Res.*, 108, 1203
- Dröge, W. 2000, *ApJ*, 537, 1073
- Earl, J. A. 1973, *ApJ*, 180, 227
- . 1976a, *ApJ*, 205, 900
- . 1976b, *ApJ*, 206, 301
- Jokipii, J. R. 1966, *ApJ*, 146, 480
- . 1971, *Rev. Geophys. Space Phys.*, 9, 27
- Jokipii, J. R. & Coleman, Jr., P. J. 1968, *J. Geophys. Res.*, 73, 5495
- Kahler, S. W., Reames, D. V., & Sheeley, Jr., N. R. 1990, in *Proc. 21st Int. Cosmic Ray Conf.*, Vol. 5, 183–186
- Kallenrode, M.-B. & Wibberenz, G. 1990, in *Proc. 21st Int. Cosmic Ray Conf.*, Vol. 5, 229–232
- Khumlumlert, T. 2001, Ph.D. thesis, Chulalongkorn University, Bangkok, Thailand
- Krucker, S., Larson, D. E., Lin, R. P., & Thompson, B. J. 1999, *ApJ*, 519, 864
- Krucker, S. & Lin, R. P. 2000, *ApJ*, 542, L61
- Leerungnavarat, K., Ruffolo, D., & Bieber, J. W. 2003, *ApJ*, 593, 587

- Lin, R. P., Potter, D. W., Gurnett, D. A., & Scarf, F. L. 1981, *ApJ*, 251, 364
- Lintunen, J. & Vainio, R. 2004, *A&A*, 420, 343
- Ng, C. K. & Wong, K.-Y. 1979, in *Proc. 16th Int. Cosmic Ray Conf.*, Vol. 5, 252
- Nutaro, T., Riyavong, S., & Ruffolo, D. 2001, *Comp. Phys. Comm.*, 134, 209
- Palmer, I. D. 1982, *Rev. Geophys. Space Phys.*, 20, 335
- Parker, E. N. 1958, *ApJ*, 128, 664
- Reames, D. V., von Rosenvinge, T. T., & Lin, R. P. 1985, *ApJ*, 292, 716
- Reiner, M. J. & Stone, R. G. 1988, *A&A*, 206, 316
- . 1989, *A&A*, 217, 251
- Roelof, E. C. 1969, in *Lectures in High Energy Astrophysics*, ed. H. B. Ögelman & J. R. Wayland, NASA SP-199 (Washington, D.C.: NASA), 111–135
- Ruffolo, D. 1995, *ApJ*, 442, 861
- Ruffolo, D., Khumlumlert, T., & Youngdee, W. 1998, *J. Geophys. Res.*, 103, 20591
- Tylka, A. J. et al. 2003, in *Proc. 28th Int. Cosmic Ray Conf.*, Vol. 6, 3305
- Valdés-Galicia, J. F., Wanner, W., Kallenrode, M.-B., & Wibberenz, G. 1995, *ApJ*, 439, 482

Table 1. Results of the inverse velocity fits

λ_0^a (AU)	α	Injection	Duration	Threshold (% of peak)	$t_{\text{inj}} - t_0$ (min)	s (AU)	$\chi^2/(N - 2)$ (min ²)
1.0	-1/3	Impulsive	–	0.01	1.52	1.16	0.39
1.0	-1/3	Extended	Constant	0.01	2.98	1.16	0.96
1.0	-1/3	Extended	Variable	0.01	2.28	1.20	0.58
1.0	0	Impulsive	–	0.01	0.62	1.17	0.16
1.0	0	Extended	Constant	0.01	1.41	1.18	1.07
1.0	0	Extended	Variable	0.01	0.70	1.21	0.26
0.2	0	Impulsive	–	0.01	0.76	1.31	0.27
0.2	0	Extended	Constant	0.01	2.54	1.35	1.35
0.2	0	Extended	Variable	0.01	1.25	1.43	0.94
0.2	1/3	Impulsive	–	0.01	-0.99	1.32	0.04
0.2	1/3	Extended	Constant	0.01	-0.13	1.36	0.19
0.2	1/3	Extended	Variable	0.01	-1.45	1.44	0.03
0.2	1	Impulsive	–	0.01	-3.46	1.33	2.00
0.2	1	Extended	Constant	0.01	-3.58	1.38	1.31
0.2	1	Extended	Variable	0.01	-5.68	1.46	3.87
1.0	-1/3	Impulsive	–	2.0	1.94	1.19	0.21
1.0	-1/3	Extended	Constant	2.0	5.64	1.21	1.13
1.0	-1/3	Extended	Variable	2.0	3.97	1.32	2.03
1.0	0	Impulsive	–	2.0	0.50	1.20	0.09
1.0	0	Extended	Constant	2.0	2.80	1.23	0.91
1.0	0	Extended	Variable	2.0	1.14	1.34	0.75
0.2	0	Impulsive	–	2.0	0.91	1.41	0.39
0.2	0	Extended	Constant	2.0	5.16	1.46	2.32
0.2	0	Extended	Variable	2.0	1.99	1.67	2.32
0.2	1/3	Impulsive	–	2.0	-1.82	1.43	0.15
0.2	1/3	Extended	Constant	2.0	1.30	1.49	0.66
0.2	1/3	Extended	Variable	2.0	-1.82	1.69	0.12
0.2	1	Impulsive	–	2.0	-5.92	1.45	6.84
0.2	1	Extended	Constant	2.0	-4.34	1.52	2.00
0.2	1	Extended	Variable	2.0	-8.56	1.73	6.05

Table 1—Continued

λ_0^a (AU)	α	Injection	Duration	Threshold (% of peak)	$t_{\text{inj}} - t_0$ (min)	s (AU)	$\chi^2/(N - 2)$ (min ²)
1.0	−1/3	Impulsive	–	60.0	3.99	1.25	0.93
1.0	−1/3	Extended	Constant	60.0	14.54	1.26	2.41
1.0	−1/3	Extended	Variable	60.0	7.26	1.75	13.81
1.0	0	Impulsive	–	60.0	0.69	1.27	0.22
1.0	0	Extended	Constant	60.0	10.47	1.29	1.42
1.0	0	Extended	Variable	60.0	3.39	1.78	8.06
0.2	0	Impulsive	–	60.0	1.31	1.66	0.79
0.2	0	Extended	Constant	60.0	12.90	1.66	1.05
0.2	0	Extended	Variable	60.0	4.82	2.22	15.35
0.2	1/3	Impulsive	–	60.0	−2.72	1.68	0.07
0.2	1/3	Extended	Constant	60.0	7.51	1.70	0.26
0.2	1/3	Extended	Variable	60.0	−0.42	2.24	4.46
0.2	1	Impulsive	–	60.0	−10.70	1.72	11.45
0.2	1	Extended	Constant	60.0	−0.74	1.74	5.42
0.2	1	Extended	Variable	60.0	−7.92	2.27	2.74

^aRadial mean free path at a proton kinetic energy of 2 MeV (or a electron kinetic energy of ≈ 1 keV, see text).

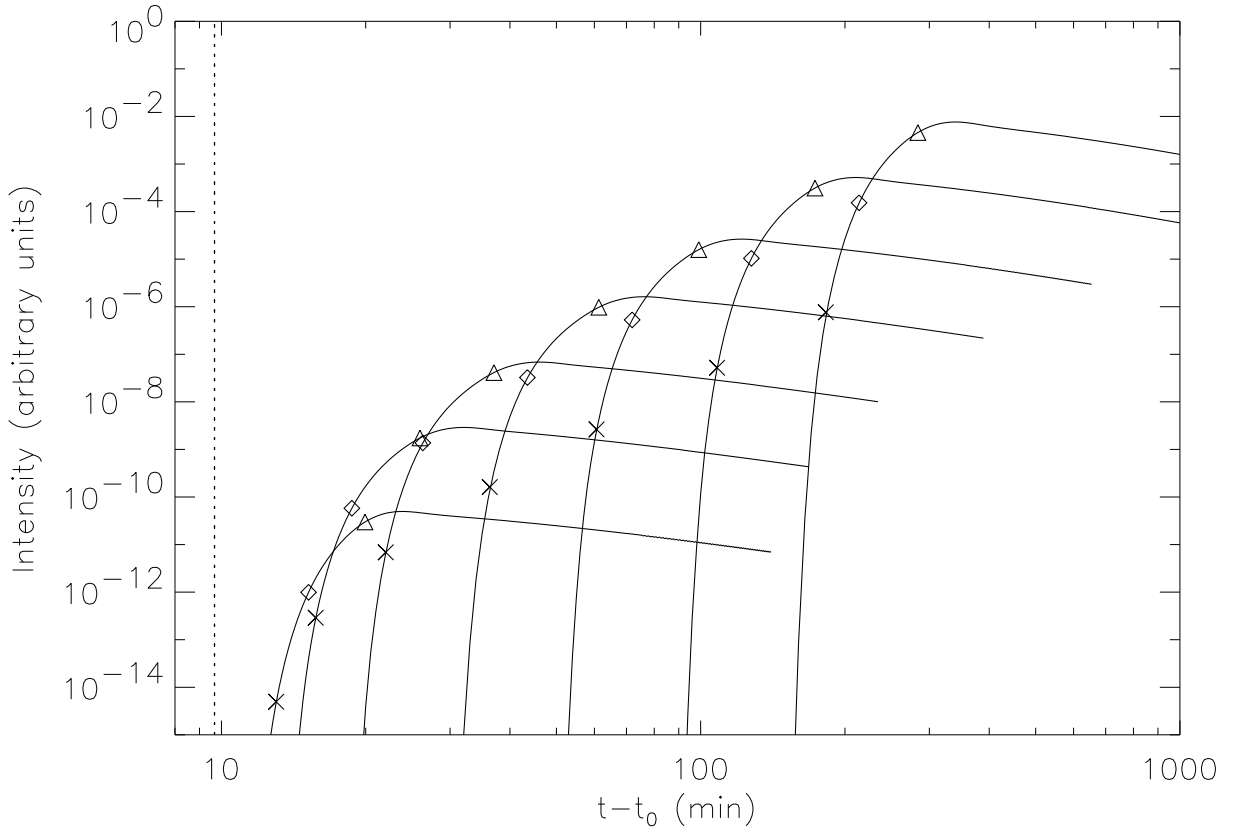


Fig. 1.— Time profiles for the intensity at Earth orbit of protons of different energies, resulting from an extended injection near the Sun with a duration dependent on proton energy, and for a constant radial mean free path $\lambda_r = 0.2$ AU. The vertical dotted line denotes the time at which particles travelling directly along the magnetic field line would arrive in the limit $v \rightarrow c$. The detection times, or points where the profiles surpass a certain threshold, are marked by crosses (low threshold, 0.01% of the peak), diamonds (medium threshold, 2% of the peak), and triangles (high threshold, 60% of the peak).

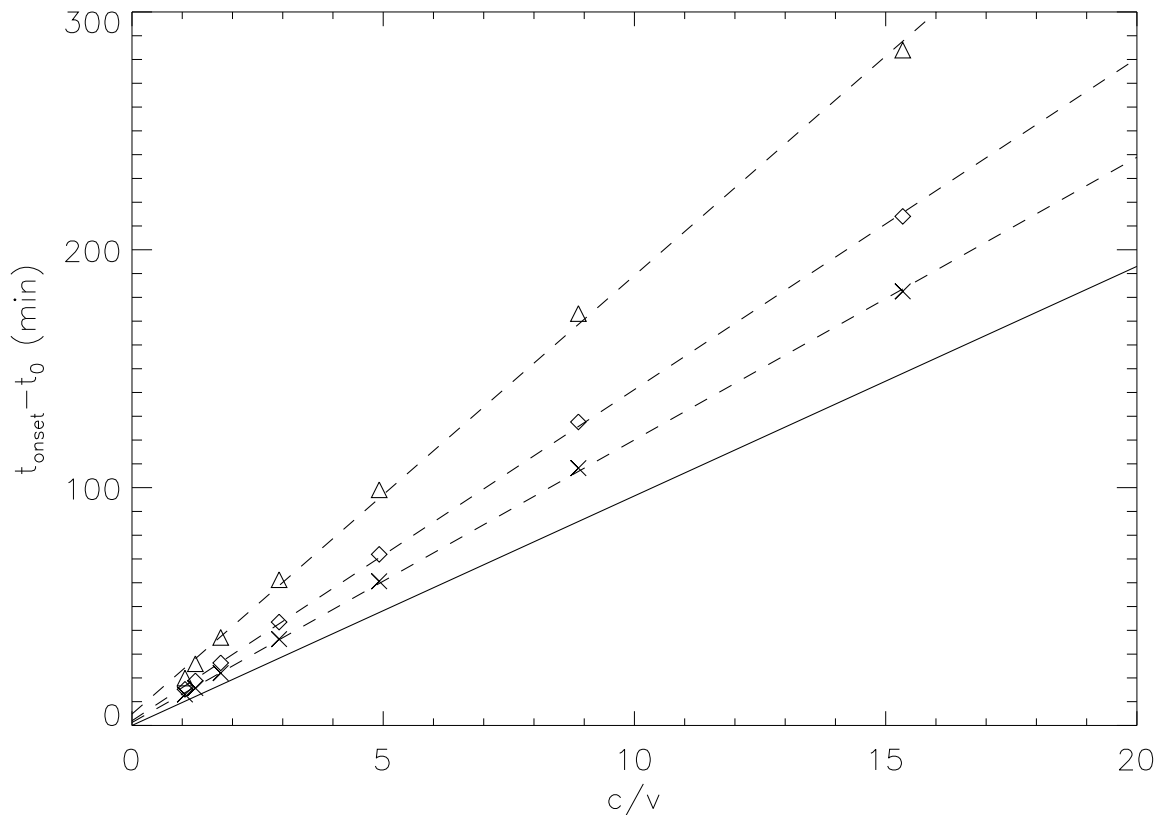


Fig. 2.— Inverse velocity fit to the onset times of protons of different energies, deduced for the case shown in Figure 1, showing all three threshold assumptions. The linear fits (dashed lines) correspond to $1.25 \text{ min} + 1.43 \text{ AU}/v$ for the low threshold (crosses, 0.01% of the peak), $1.99 \text{ min} + 1.67 \text{ AU}/v$ for the medium threshold (diamonds, 2% of the peak), and $4.82 \text{ min} + 2.22 \text{ AU}/v$ for the high threshold (triangles, 60% of the peak). The solid line is $0.00 \text{ min} + 1.16 \text{ AU}/v$, i.e., where points would line up if particles could travel directly along the magnetic field without any scattering.

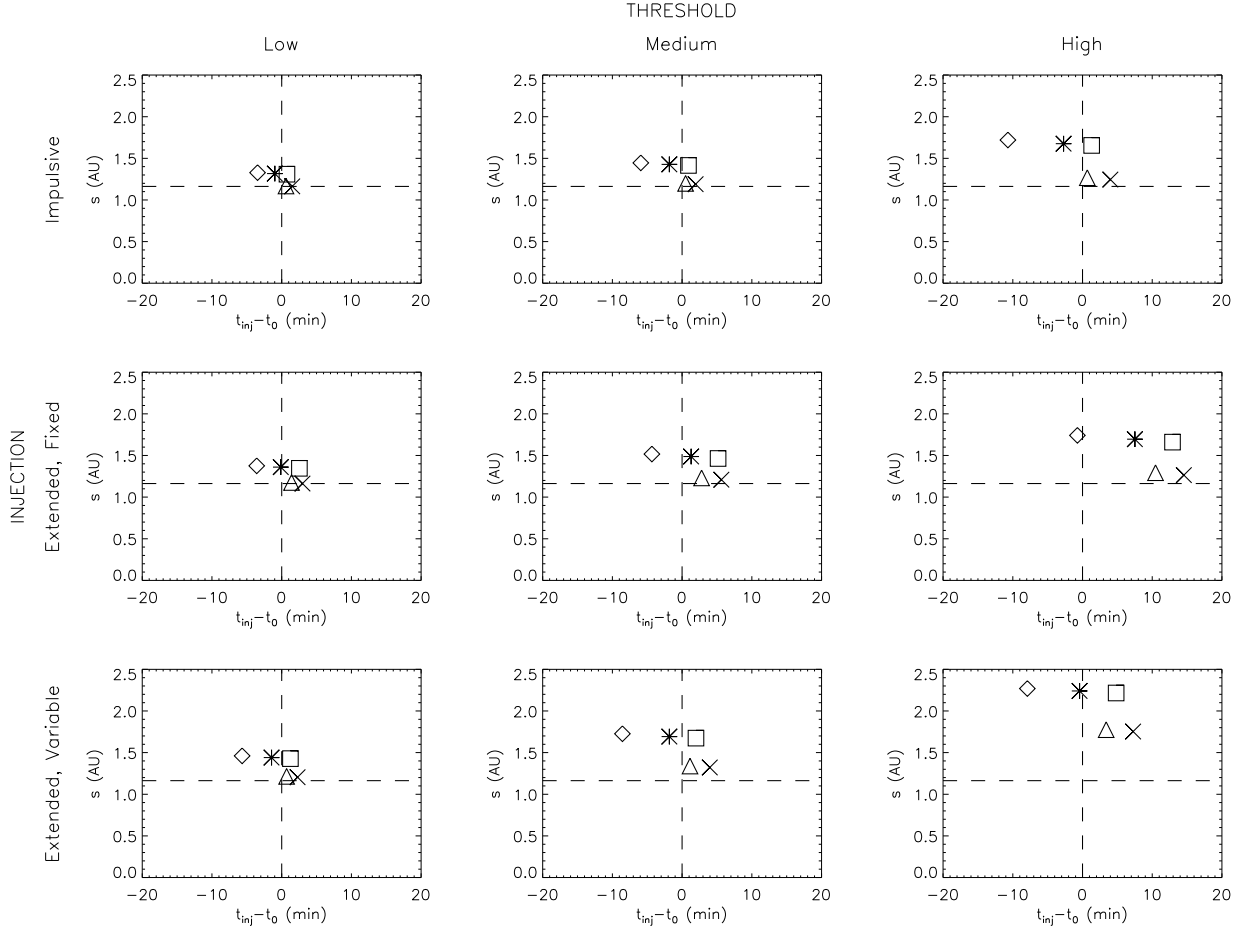


Fig. 3.— Times of injection vs. path lengths estimated from the inverse velocity fits in the different cases studied. Left panels: results of the low threshold assumption (0.01% of the peak). Center panels: results of the medium threshold assumption (2% of the peak). Right panels: results of the high threshold assumption (60% of the peak). Top panels: impulsive injection. Middle panels: extended injection with constant absolute width (12 min). Bottom panels: extended injection with width depending on particle rigidity (see text). Different symbols denote different mean free path assumptions: crosses: $\lambda_0 = 1.0$ AU, $\alpha = -1/3$; triangles: $\lambda_0 = 1.0$ AU, $\alpha = 0$; squares: $\lambda_0 = 0.2$ AU, $\alpha = 0$; stars: $\lambda_0 = 0.2$ AU, $\alpha = 1/3$; diamonds: $\lambda_0 = 0.2$ AU, $\alpha = 1$. The intersection of dashed lines indicates the actual values of the start time of injection and path length used in performing all the simulations.